Acta Geochim (2019) 38(5):670–682
https://doi.org/10.1007/s11631-019-00362-w

ORIGINAL ARTICLE

Fluid properties and sources of Sixiangchang carbonate-associated mercury deposit, southwest China

Yuzhou Zhuo[1,2] · Yong Huang[1,2] · Jinwei Li[1,2] · Wei Gao[1,2] · Jinxiang Li[1,2]

Received: 8 March 2019 / Revised: 6 June 2019 / Accepted: 27 June 2019 / Published online: 4 July 2019

Abstract Mercury mines in Guizhou province are the main base of mercury production and the most important resource base in China. The San-Dan mercury belt in Guizhou province contains a series of important mercury deposits. However, the source of metallogenic materials and the properties of metallogenic fluid of these mercury deposits have long been a controversial issue. In this study, we used cathode luminescence techniques to distinguish different stages of dolomite and calcite, laser ablation inductively coupled plasma mass spectrometry to analyze the trace elements, and stable isotope mass spectrometry techniques to analyze C–O isotopes compositions of dolomite and calcite in the Sixiangchang mercury deposit in San-Dan mercury belt. We also measured the sulfur isotope composition of cinnabar. Our study showed that dolomite can be divided into two stages, the lumpy dolomite associated with cinnabar in Dol 1 stage and dolomite vein in Dol 2 stage, which is associated with Cal 2 stage calcite vein. With the progress of mineralization, Al, As, Mo, Sb, and Sr elements were gradually enriched in the ore-forming fluid. The rare earth element (REE) partition curve of Dol 1 stage dolomite showed a trend of light REE enrichment. Cal 2 stage calcite and Dol 2 stage dolomite exhibited a flat-type REE partition curve, and Dol 2 stage dolomite showed a strong negative anomaly for Eu. $\delta^{13}C$ of carbonate mineral variation ranges from − 6.89 to − 2.16 ‰, while $\delta^{18}O$ variation ranges from 13.80 to 23.09 ‰, and the $\delta^{34}S$ variation range of cinnabar is 16.51–24.28 ‰. Carbonate mineral trace elements and C–O isotopes compositions suggested that early ore-forming fluid was reduced, and late ore-forming fluid was oxidized. The ore-forming fluid of the Sixiangchang mercury deposit is a mixture of deep crustal fluid and meteoric water in deep thermal circulation, and involved in the oxidation of organic matter. The cinnabar $\delta^{34}S$ results showed that sulfur mainly came from seawater sulfate with the participation of microbial reduction. Sulfur is sedimentary in origin and was derived mainly from the host-rock strata.

Keywords Trace elements · Carbon and oxygen isotopes · Sulfur isotope · Calcite and dolomite · Youjiang Basin

1 Introduction

The distribution of mercury resource is extremely uneven, with three-quarters of global mercury production comes from five major mercury mining zones (Rytuba 2003). The Almaden mercury belt of central Spain alone accounts for one-third of the world's mercury production (Saupe 1990). There are many genetic types of mercury deposit. Rytuba (2003) suggested that mercury mine could be divided into three types: silica-carbonate, hot-spring, and Almaden. China is rich in mercury resource, and mercury deposits are distributed throughout the country. Guizhou province is the most abundant province of mercury resources in China (He 1990). In Guizhou province, the San-Dan mercury ore belt is the most important mercury ore belt. It is located in the northeast of the Guizhou province. San-Dan mercury ore belt is an important area of mercury and an important part

✉ Yuzhou Zhuo
zhuoyuzhou163@163.com

[1] State Key Laboratory of Ore Deposit Geochemistry, Institute of Geochemistry, Chinese Academy of Sciences, Guiyang 550081, China

[2] College of Earth and Planetary Sciences, University of Chinese Academy of Sciences, Beijing 100049, China

of the large area of low-temperature mineralization in southwest China (Yan et al. 1989).

As a kind of unique mineralization type, mercury deposits in southwest China have their own distinct geochemical characteristics. Carbonate is the main host-rock and the ore deposit is obviously strata-bound (Cambrian, Ordovician). The metallogenic age is Yanshanian, and the cause has nothing to do with magmatic rocks such as the difference between the other types of mercury (Wang and Wen 2015). Therefore, research of the mercury deposit in southwest China has high significance (Yan et al. 1989). However, the source of metallogenic materials and the properties of ore-forming fluid have long been a controversial issue. Some scholars researched C and O isotopes of calcite, Pb and S isotopes of sulfide, and their result suggested that the ore-forming fluid of the mercury mine was related to the hydrocarbon brine containing organic matter in the ancient reservoir (Bao et al. 1999; Shi 1991; Li et al. 2002; Wang and Gao 2017). Yan et al. (1989) through field geological observation and mercury concentration test in host-rock suggested that the mercury mainly comes from the host-rock. However, previous studies mainly focused on the study of field geology, and ignored the division of metallogenic stage. The studies did not have detailed mineralogical research, and published data of isotopes and trace elements were very few.

In recent years, with the development of microanalysis technology, there have been a lot of studies on the geochemical study of pyrite and quartz in Carlin-type gold deposit (Hu and Zhou 2012; Hu et al. 2017; Su et al. 2009, 2018). However, these analytical techniques are rarely used in the study of mercury deposit. In this study, we use laser ablation inductively coupled plasma mass spectrometry (LA-ICP-MS) technique in conjunction with textural studies utilizing the cathode luminescence (CL) technique to measure the trace elements of calcite and dolomite in different mineralization stage of Sixiangchang deposit in the San-Dan metallogenic belt. We measured $\delta^{13}C$ and $\delta^{18}O$ in different stages of calcite and dolomite, and measured $\delta^{34}S$ of cinnabar. The goal of this study is to document the sources and properties of the ore-forming fluid of the Sixiangchang mercury deposit, and trace the source of S element. Our new data provide evidence of the properties and sources of ore-forming fluid.

2 Regional geology

The San-Dan metallogenic belt is located in the northeast margin of Youjiang basin, Southwest China (Fig. 1). This metallogenic belt resides at the junction of Yangtze craton and the South China fold belt (Huang and Du 1993). The Sixiangchang mercury deposit is located in the middle of the San-Dan metallogenic belt (Fig. 1) (Huang and Du 1993), which is in the northeastern margin of the Youjiang basin. The Youjiang basin is bound to the northeast by the Shuicheng-Ziyun-Bama fault, southwest by the Mile-Shizong fault and Nanpanjiang fault, and to the southeast by the Youjiang fault, which separates the Youjiang basin from the Cathaysia block (Su et al. 2008, 2012, 2018). The San-Dan metallogenic belt is 150 km long and 20–30 km wide, which have Sixiangchang, Shuiyinchang, Hongfachang, Jiaoli and other dozens of mineral deposits (Lei et al. 2012). Many mineral deposits have been exhausted. The main strata exposed in this area are the Cambrian basement, and Paleozoic and Triassic strata (Fig. 1). The lithology of Cambrian basement is mainly blastopsammite and siliceous rock. Paleozoic and Triassic strata lithology is limestone, sandstone, siltstone, shale, and dolomite (Hu et al. 2002). The age of Rb–Sr in the whole rock of Carlin-type gold deposit tested by Jia et al. (1993) in Danzhai Hongfachang was 400 and 114 Ma. Wang et al. (2015) researched the Sm–Nd isotopes of calcite in Danzhai Jiaoli mercury deposit, and obtained the isochronic age was 129 ± 20 Ma. They suggested that the deposit was formed in the late Yanshanian Period. Magmatic activity in this area is very weak. Granite plutons with ages varying from Triassic (or Indosinian) to Jurassic-Cretaceous (or Yanshanian) are present at the southwest margin of Youjiang Basin (Hu et al. 2002, 2017; Hu and Zhou 2012). Variscan and Indosinian diabase are deposited in the southeast of the basin (Du et al. 2013). Variscan and Indosinian mafic dyke are deposited in the part of the basin (Du et al. 2013) (Fig. 1).

3 Geological characteristics of the deposit

The Sixiangchang mercury deposit is located at the passive edge of the Yangtze plate, southeast of Guizhou province, and contains Sandu-Danzhai mercury, antimony, gold and arsenic polymetallic mineralization (Xie et al. 2014). The main element of the Sixiangchang deposit is mercury, and the auxiliary element is gold, in which the average grade of gold is 7.19 g/t (Huang and Du 1993).

The oldest strata in this area composed of the Proterozoic Xiajiang group, which is distributed in the eastern part of the mining area (Li et al. 2013) (Fig. 2). Xiajiang group lithology is mainly blastopsammite and sandy slate. The Sinian strata also distributed in the eastern part of the deposit, and the lithology is mainly carbonaceous shale, dolomite, and sandy slate. Cambrian strata are the main ore-bearing host-rock of the deposit, in which the lower and middle Cambrian lithology is mainly dolomite and limestone, and the upper Cambrian lithology is clay shale, carbonaceous shale, and limestone. The upper Cambrian

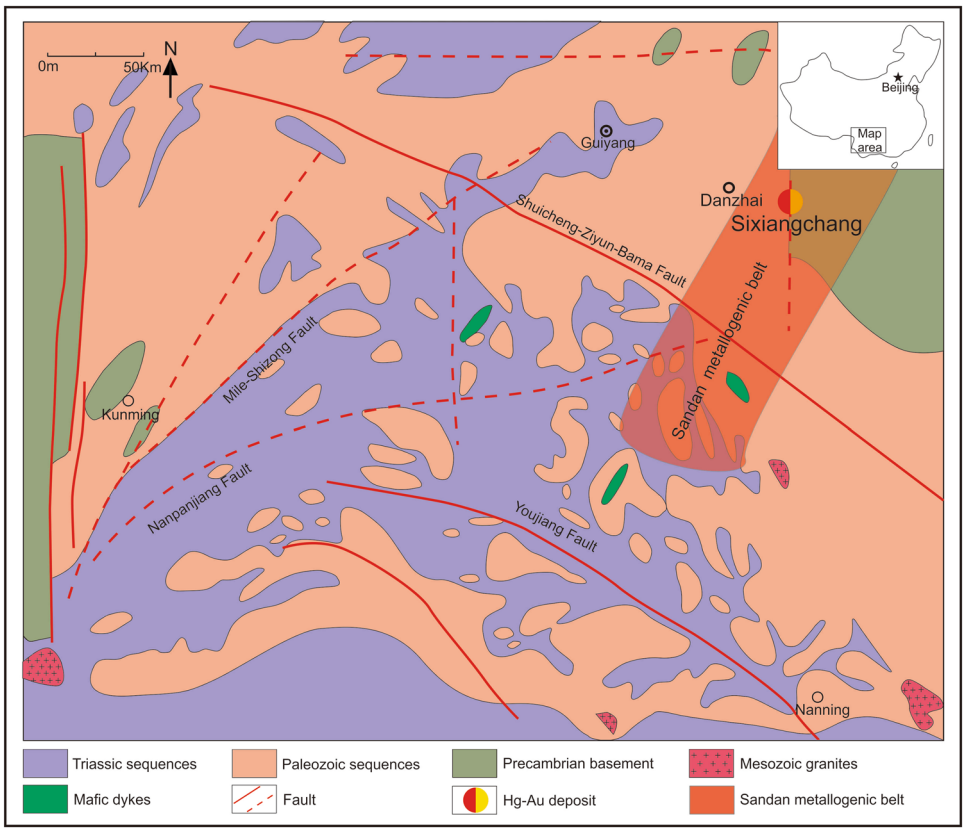

Fig. 1 Geologic map of the southwestern China, showing the location of the Sixiangchang mercury deposit in the Youjiang Basin. Modified from Hu and Zhou (2012)

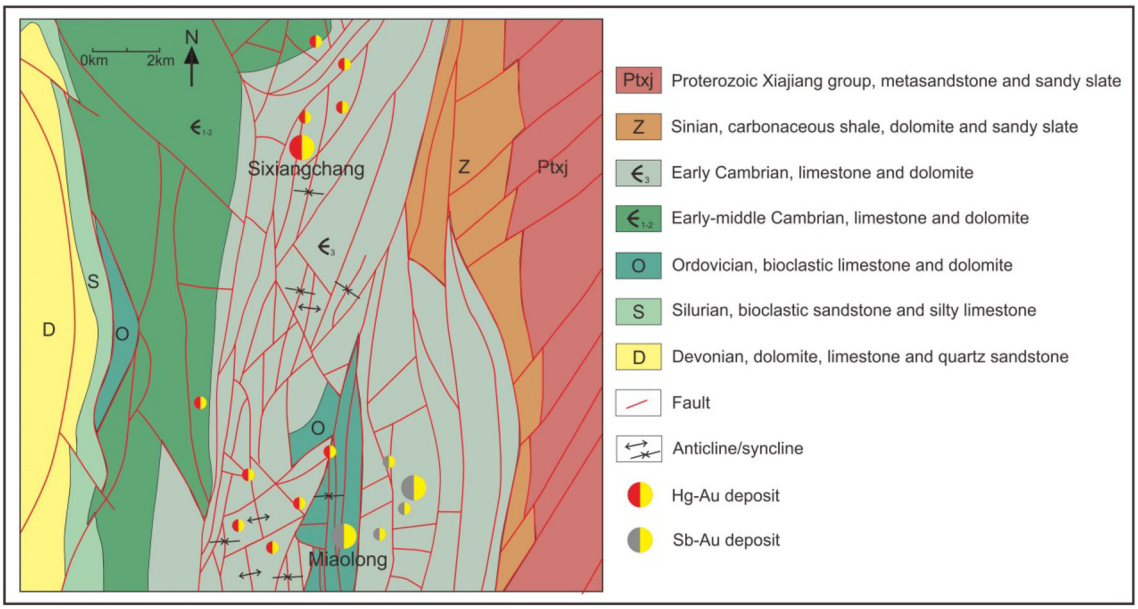

Fig. 2 Geological map of the Sixiangchang mercury deposi. Modified from Huang and Du (1993)

Yangjiawan formation is the main ore-bearing strata. The Ordovician strata are mostly missing due to tectonic activity and the lithology of the remaining strata is mainly bioclastic limestone and dolomite. Silurian strata are distributed in the western side of the mining area (Fig. 2), with a lithology of sandstone and limestone. Devonian strata are also distributed in the western side of the deposit, and the lithology is dolomite, limestone, and quartz sandstone (Yan et al. 1989). The ore minerals in the Sixiangchang mercury deposit are mainly composed of

cinnabar, pyrite, natural mercury, and stibnite (Figs. 3f, d, 4c, i), and the gangue minerals are mainly quartz, calcite, and dolomite (Figs. 3a, c, 4a, f). The alteration of the host-rock primarily includes silicification (Fig. 4f), pyritization (Fig. 4c), and dolomitization (Fig. 4e). There is strong tectonic activity in the mining area, which belongs to the multi-twist structure of the different grades of the neo-cathaysian system (Lei et al. 2012). Faults, folds, and other structural phenomena in the area are complex and changeable, with the multi-character structure being the most developed and the meridional structural movement as the main structure (Fig. 2) (Huang and Du 1993). There is no magmatic rock outcrop in the mining area.

4 Sample description and analytical methods

4.1 Sample description

Our samples for experimental analyze are from outcrops and ores in the mine pits of Sixiangchang mercury deposit. Twenty-seven samples were used for trace elements and isotopes analysis. The main lithology of the samples is sandstone, siltstone, and calcareous siltstone (Table 2). The carbonate mineral in the samples was lumpy and veined. The cinnabar in the samples is intergrowth with calcite and dolomite (Fig. 3). Six rock slice samples were used for the analysis of carbonate mineral trace elements. The trace elements of calcite and dolomite were analyzed on rock slice by the LA-ICP-MS method. Sixteen samples were used for carbonate mineral $\delta^{13}C$ and $\delta^{18}O$ analysis. Seventeen cinnabar samples were used for the analysis of $\delta^{34}S$. The carbonate mineral and cinnabar was crushed to 40–60 mesh and rinsed with ultrapure water. The impurity will be removed, so that the mineral purity of more than 99 %, then dry the samples and grind the pure carbonate mineral and cinnabar in an agate mortar until it is less than 200 mesh. Finally, analyzed $\delta^{13}C$, $\delta^{18}O$ and $\delta^{34}S$ of these carbonate mineral and cinnabar samples.

4.2 Cathode luminescence

The cathode luminescence was conducted at the State Key Laboratory of Ore Deposit Geochemistry (SKLODG) of the Institute of Geochemistry, Chinese Academy of Sciences (IGCAS) in Guiyang, China, using a Reliotron luminoscope (produced by America Relion industries use). The luminoscope was operated with an accelerating

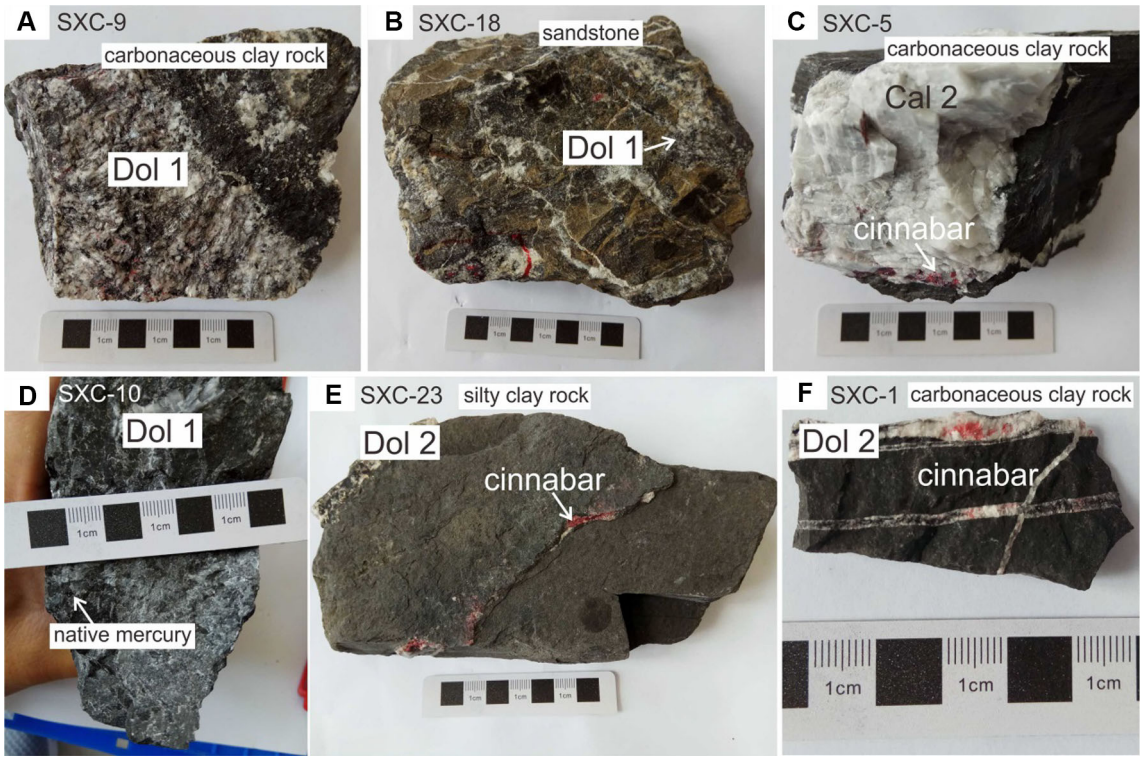

Fig. 3 The hand specimens of calcite and dolomite at different stages collected from Sixiangchang mercury deposit. **a** Carbonaceous clay rock sample with disseminated cinnabar and Dol 1 stage dolomite. **b** Sandstone sample with disseminated cinnabar and Dol 1 stage dolomite. **c** Carbonaceous clay rock sample with symbiosis cinnabar and Cal 2 stage calcite vein. **d** Carbonaceous siltstone sample with Dol 1 stage dolomite and natural mercury. **e** Silty clay sample with Dol 2 stage dolomite vein associated with cinnabar. **f** Carbonaceous clay sample with Dol 2 stage dolomite vein associated with cinnabar

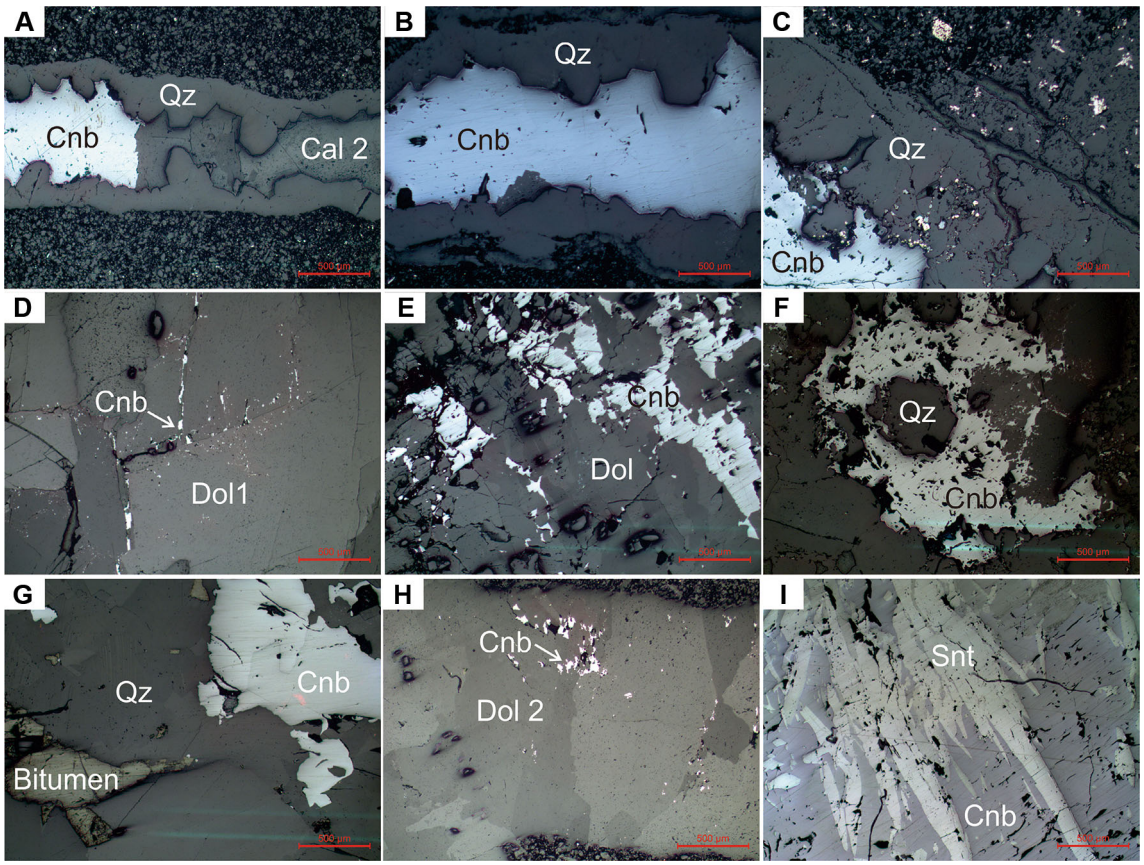

Fig. 4 The microscopic mineral photos (with a Leica DM 2500 P microscope) of calcite and dolomite at different stages collected from Sixiangchang mercury deposit. **a** Cal 2 stage calcite vein associated with cinnabar is embedded in quartz vein. **b** Quartz vein contains veined cinnabar. **c** Cinnabar, pyrite, and quartz symbiosis. **d** Dol 1 stage dolomite fractures are filled with fine cinnabar. **e** Cinnabar is disseminated in the Dol 1 stage dolomite. **f** Quartz and cinnabar grains are encapsulated and encased. **g** Cinnabar particles and bitumen embedded in quartz particles. **h** Dol 2 stage dolomite vein contain fine cinnabar. **i** Cinnabar and stibnite are symbiotic. *Qz* quartz, *Cal* calcite, *Cnb* cinnabar, *Dol* dolomite, *Snt* stibnite

voltage of 5 kV, a current of 500 μA, and a vacuum degree of 80–90 mTorr (Wei et al. 2015).

4.3 LA-ICP-MS

Calcite trace elements were analyzed at the SKLODG of the IGCAS. Laser sampling was performed using a GeoLas Pro 193 nm ArF excimer laser (produced by Germany Coherent). An Agilent 7500× ICP-MS instrument (produced by Agilent) was used to acquire ion-signal intensities. Helium was applied as a carrier gas which was mixed with Argon via a T-connector before entering the ICP-MS. Each analysis incorporated a background acquisition of approximately 30 s (gas blank) followed by 50 s of data acquisition from the sample.

The trace elements tested in this experiment include Li, Be, B, Na, Mg, Al, Si, P, K, Sc, Ti, V, Cr, Mn, Fe, Co, Ni, Cu, Zn, Ga, Ge, As, Rb, Sr, Y, Zr, Nb, Mo, Ag, Cd, Sn, Sb, Cs, Ba, Hf, Ta, Au, Pb, Th, U and REE. If the concentrations of analyzed elements are < 0.1 μg/g, we considered the analyzed results unreliable. Element concentration was calibrated against multiple-standard reference materials (NIST 610, NIST 612) (Jochum et al. 2015) combined with carbonate reference material MACS-3 as internal standardization. The parameters of the reference material are shown in the literature (Chen et al. 2011; Jochum et al. 2012). The laser ablation frequency was 5 Hz, the laser beam spot was 44 μm. A set of standard samples was tested after 10 sample points finished, with an analysis error of less than 10 %. Off-line selection and integration of background and analyte signals, and time-drift correction and quantitative calibration were performed by ICPMSDataCal (Liu et al. 2008, 2010).

4.4 Stable isotopes

4.4.1 C–O isotopes analysis of calcite and dolomite

Calcite and dolomite carbon and oxygen stable isotopes were conducted at the SKLODG of the IGCAS. Carbon

and oxygen stable isotopes were carried out with a ThermoFisher MAT 253 mass spectrometer (produced by America ThermoFisher). The samples were reacted with 100 % concentrated H_3PO_4 in a vacuum at 72 °C for 12 h. The released CO_2 was analyzed for carbon and oxygen isotopes. Isotopic data are reported in ‰ relative to the Peer Dee Belemnite (PDB) for carbon and oxygen. The following standards were used for internal calibration standards: GBW04416 (calcite, $\delta^{13}C_{PDB} = 1.61$ ‰, $\delta^{18}O_{PDB} = -11.59$ ‰), GBW04405 (calcite, $\delta^{13}C_{PDB} = 0.57$ ‰, $\delta^{18}O_{PDB} = -8.49$ ‰), NBS18 (calcite, $\delta^{13}C_{PDB} = -5.01$ ‰, $\delta^{18}O_{PDB} = -23.2$ ‰) and L-SVEC (lithiumcarbonate, $\delta^{13}C_{PDB} = -46.6$ ‰, $\delta^{18}O_{PDB} = -26.7$ ‰). The analytical precision at 2σ for $\delta^{13}C$ and $\delta^{18}O$ are ± 0.2 and ± 2.0 ‰, respectively (Zhou et al. 2017). The $\delta^{13}C$ and $\delta^{18}O$ test results are shown in Table 1. The values of $\delta^{18}O_{SMOW}$ (Vienna Standard Mean Ocean Water) were calculated based on the equation of Friedman and O'Neil (1977), where $\delta^{18}O_{SMOW} = 1.03086 \times \delta^{18}O_{PDB} + 30.86$.

4.4.2 S isotope analyze of cinnabar

The sulfur isotope of cinnabar was analyzed at the SKLODG of the IGCAS. Cinnabar with a purity of greater than 99 % was selected and ground to 200 mesh in agate mortars. A sample in a foil package was put into a small bottle before testing. Sulfides were combusted with copper oxide under vacuum at 1000 °C to produce SO_2 which was used for the gas mass spectrometer measurements (Robinson and Kusakabe 1975). The cinnabar $\delta^{34}S$ was analyzed with the ThermoFisher MAT253 stable isotope mass spectrometer. Isotopic data were reported as $\delta^{34}S$ relative to IAEA-S-1 ($\delta^{34}S_{VCDT} = -0.30$ ‰), IAEA-S-2 ($\delta^{34}S_{VCDT} = 22.62$ ‰) and IAEA-S-3 ($\delta^{34}S_{VCDT} = -32.49$ ‰) standards for sulfur (Zhou et al. 2017). The relative error at 2σ was better than 0.1 ‰. The sulfur isotope test results are shown in Table 2.

5 Results

5.1 Cathode luminescence characteristics and stage division of calcite and dolomite

The carbonate minerals in the Sixiangchang mercury deposit are dolomite and calcite, but primarily dolomite. According to hand specimens and microscopic mineral assemblage observations, dolomite is divided into two stages, Dol 1 stage and Dol 2 stage, and calcite is characterized as Cal 2 stage. Dol 1 stage dolomite is primarily in the form of milky clumps and is distributed in the host-rock in an infective form with cinnabar (Figs. 3a, b, 4d). Dol 1 stage dolomite glows a bright red under cathode luminescence (Fig. 5b, c), and dark in the area with high Fe concentration (Fig. 5a, points 1 and 4). Dol 2 stage dolomite has milky white veins with cinnabar (Fig. 3e, f). Dol 2 stage dolomite glows dark under cathode luminescence

Table 1 Carbon and oxygen isotopes compositions and calculated temperatures of carbonate mineral in Sixiangchang mercury deposit

Sample (ID)	Lithology	Stage	$\delta^{13}C(‰_{V\text{-}PDB})$	$\delta^{18}O(‰_{SMOW})$	$\delta^{13}C$ $‰_{CO2}$	$\delta^{18}O$ $‰_{H2O}$	Temperature (°C)
SXC-5	Carbon mudstone	Cal 2	− 6.13	18.93	− 7.08	6.80	150
SXC-6	Siltstone	Dol 2	− 2.43	20.68	− 3.38	8.54	150
SXC-7	Siltstone	Dol 2	− 5.30	18.70	− 6.25	6.56	150
SXC-9	Sandstone	Dol 1	− 3.24	19.51	− 2.49	10.48	200
SXC-10	Siltstone	Dol 1	− 2.16	19.15	− 1.42	10.12	200
SXC-15	Calcareous siltstone	Dol 2	− 2.27	20.33	− 3.22	8.20	150
SXC-18	Siltstone	Dol 1	− 3.12	20.04	− 2.37	11.01	200
SXC-21	Sandstone	Dol 1	− 2.68	21.27	− 1.93	12.25	200
SXC-24	Sandstone	Dol 2	− 3.91	20.35	− 4.87	8.22	150
SXC-26	Calcareous siltstone	Dol 2	− 6.89	23.09	− 7.84	10.96	150
SXC-27	Carbonaceous clay rock	Dol 2	− 3.13	15.77	− 4.09	3.63	150
SXC-28	Limestone	Dol 1	− 2.84	13.80	− 2.09	4.77	200
SXC-30	Carbonaceous clay rock	Dol 2	− 3.90	17.02	− 4.85	4.88	150
SXC-34	Sandstone	Dol 2	− 6.62	20.58	− 7.58	8.45	150
SXC-35	Sandstone	Dol 1	− 4.21	17.45	− 3.46	8.42	200
SXC-36	Siltstone	Dol 1	− 2.33	19.83	− 1.58	10.81	200
		Dol 1	− 4.21 ~ − 2.16	13.80–21.27	− 3.46 ~ − 1.42	4.77–12.25	
		Dol 2	− 6.89 ~ − 2.27	15.77–23.09	− 7.84 ~ − 3.22	3.63–10.96	

Table 2 Sulfur isotope composition of cinnabar in Sixiangchang mercury deposit

Smaple (ID)	Lithology	$\delta^{34}S$ (‰)
SXC-4	Carbon mudstone	23.58
SXC-5	Carbon mudstone	24.28
SXC-7	Siltstone	23.41
SXC-9	Sandstone	23.56
SXC-11	Carbon mudstone	16.51
SXC-12	Siltstone	21.66
SXC-16	Gray sandstone	21.03
SXC-18	Siltstone	18.40
SXC-20	Mudstone	22.60
SXC-22	Siltstone	22.33
SXC-23	Carbonaceous clay rock	22.91
SXC-25	Siltstone	23.64
SXC-29	Siltstone	12.08
SXC-33	Siltstone	22.82
SXC-35	Sandstone	20.41
SXC-36	Siltstone	22.87
SXC-38	Siltstone	22.81

(Fig. 5e). Cal 2 stage calcite is mainly in the form of milky white rough veins and infective with cinnabar (Figs. 3c, 4a). Cal 2 stage calcite vein glows bright red under cathode luminescence (Fig. 5a, d). The detailed sequence of mineral symbiosis is shown in Fig. 6.

5.2 Trace elements and REEs of calcite and dolomite

The concentrations of Cu, Mn and Sn in calcite and dolomite in the Sxiangchang Hg deposit have small variation ranges than Fe, Sb and Sr (Fig. 7). The elements with the highest concentrations in calcite and dolomite are Fe, Mg, Mn, Na, Si, Sr, and Al, with the concentrations ranging from tens to thousands of ppm (Fig. 7). The concentrations of Cu, Mo, Zn, As, Sb, Sn range from below the detection limit to tens of ppm. The concentrations of Sr and As in calcite are higher than dolomite, which indicates that these two elements are more likely to enter calcite.

The REE distribution forms of calcite and dolomite in Sixiangchang mercury deposit are flat and light REE enrichment (Fig. 8). The Cal 2 stage calcite exhibits a flat-

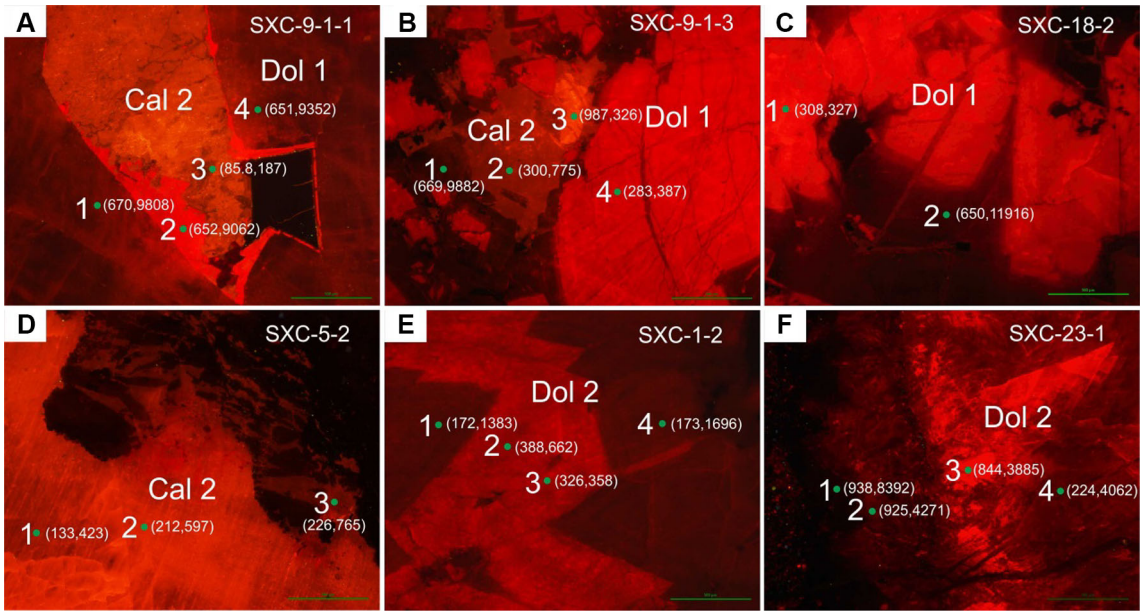

Fig. 5 The cathode luminescence photos of calcite and dolomite at different stages collected from Sixiangchang mercury deposit. (Mn, Fe) represent the concentrations of Mn and Fe of calcite and dolomite, the concentration unit is μg/g. **a** Cal 2 stage calcite glows bright red under cathode luminescence, symbiotic with Dol 1 stage dolomite, which glows dark red under the same luminescence. **a**, **b** are the cathode luminescence photos of the sample SXC-9 (Fig. 3a). **b** The red glow of Dol 1 stage dolomite. **c** Dol 1 stage dolomite glows bright red under cathode luminescence and glows dark red in local areas. **c** Cathode luminescence photo of the sample SXC-18 (Fig. 3b). **d** The bright red glow of Cal 2 stage calcite. **d** Cathode luminescence photo of the sample SXC-5 (Fig. 3c). **e** The bright red and dark red interphase of Dol 2 stage dolomite. **e** Cathode luminescence photo of the sample SXC-1 (Fig. 3f). From this cathode luminescence photo, we can see that the area of the bright red cathode light calcite tends to have a higher content of Mn and a lower content of Fe, and areas with a dark red cathode light tend to have lower levels of Mn and higher levels of Fe. **f** The bright red glow of Dol 2 stage dolomite. **f** Cathode luminescence photo of the sample SXC-23 (Fig. 3e). Cathode luminescence photos of SXC-9-1-2, SXC-18-3, SXC-5-1 and SXC-23-2 are similar with the photos of SXC-9-1-1, SXC-18-2, SXC-5-2 and SXC-23-1 respectively, so we didn't show them in the text

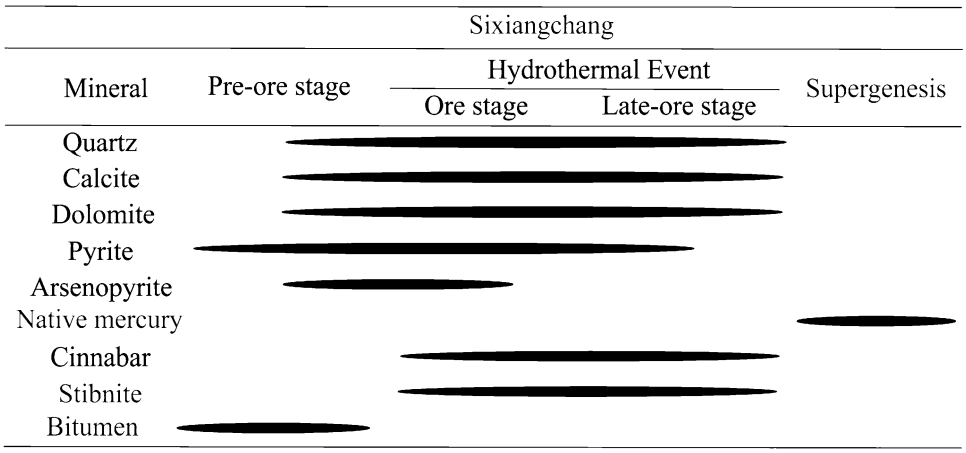

Fig. 6 Generalized alteration and ore mineral paragenesis of the Sixiangchang mercury deposit

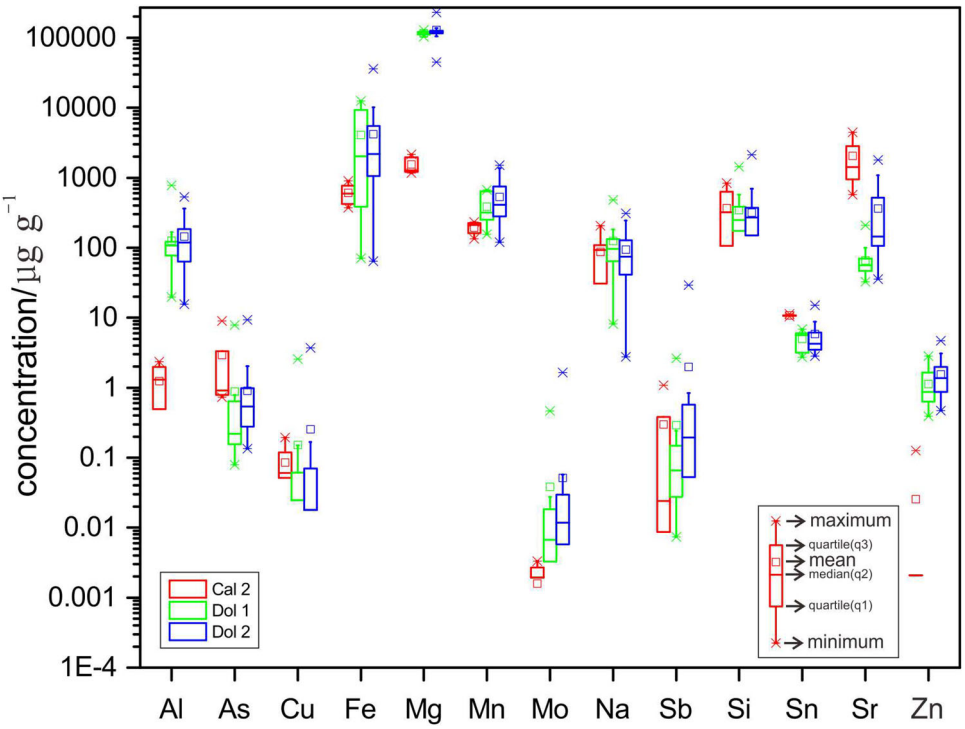

Fig. 7 Box diagram of characteristic trace elements of different stages of calcite and dolomite in Sixiangchang mercury deposit. Cal 2 is representative of Cal 2 stage calcite, Dol 1 is representative of Dol 1 stage dolomite, Dol 2 is representative of Dol 2 stage dolomite

type (Fig. 8c) REE partition curve with the ΣREE concentration varies from 16.27 ppm to 132.33 ppm. Dol 1 stage dolomite exhibits light REE enrichment (Figs. 8a, b), and the ΣREE concentration varies from 4.43 to 289.07 ppm. The REE of the Dol 2 stage dolomite are distributed in a flat pattern with a strong Eu negative anomaly (Fig. 8d–f), and the ΣREE concentration varies from 2.45 to 301.62 ppm.

5.3 C and O isotopes of calcite and dolomite

In our study, we selected 15 dolomite samples and 1 calcite sample for carbon and oxygen isotope analysis. The $\delta^{13}C$ (‰V-PDB) is in the range of − 4.21 ∼ − 2.16 ‰ in Dol 1 stage dolomite, − 6.89 ∼ − 2.27 ‰ in Dol 2 stage dolomite, and − 6.13 ‰ in Cal 2 stage calcite (Table 1). The $\delta^{18}O$ (‰S-MOW) is in the range of 13.80–21.27 ‰ in Dol 1 stage dolomite, 15.77–23.09 ‰ in Dol 2 stage dolomite, and 18.93 ‰ in Cal 2 stage calcite. According to the calcite-carbon dioxide conversion formula: $1000\ln\alpha = 2.962 - 11.346 \times 10^3/T + 5.358 \times 10^6/T^2 - 0.388 \times 10^9/T^3$ (T = 0–3727 °C) (Chacko et al. 1991) and the calcite fluid inclusion temperature data, the calcite carbon isotope can be converted into the fluid carbon dioxide carbon isotope value. $1000\ln\alpha = \delta^{13}C_{CaCO_3} - \delta^{13}C_{CO_2}$, T representative Kelvin temperature. The Dol 1 stage dolomite formation temperature is 200 °C, and the Dol 2 stage dolomite and Cal 2 stage calcite fluid inclusion

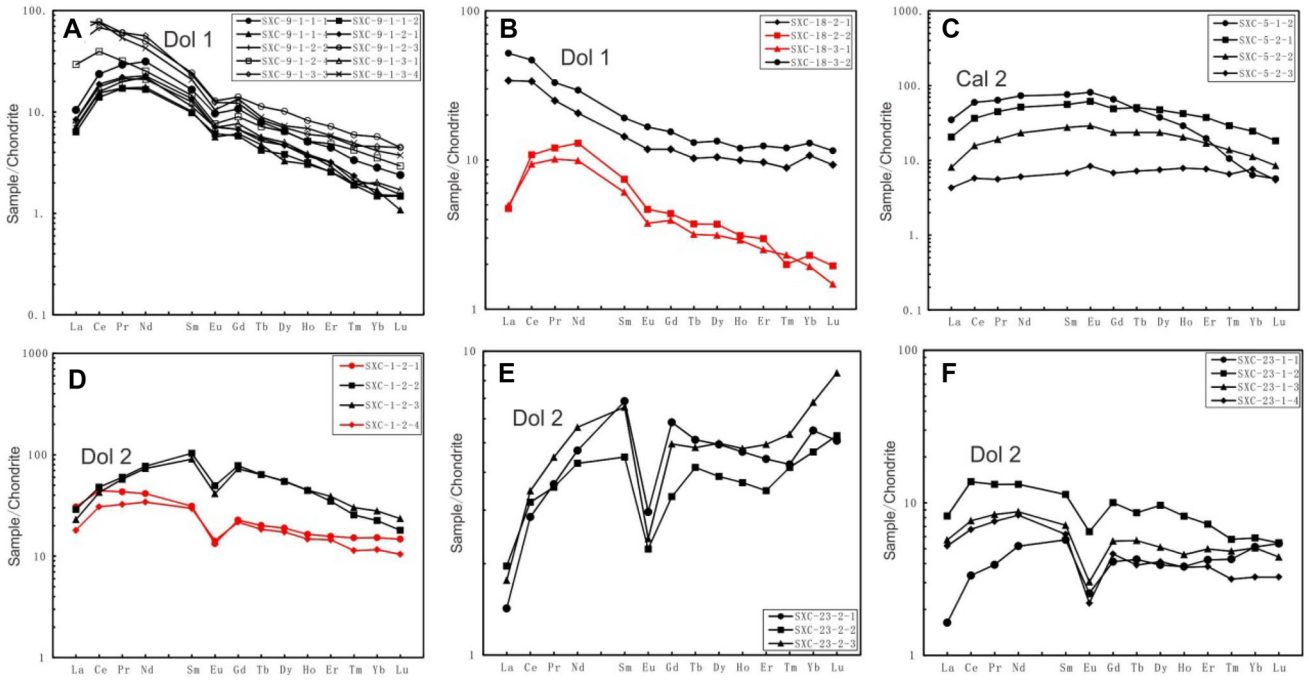

Fig. 8 Chondrite-normalized rare earth element (REE) patterns of different stages of calcite and dolomite in the Sixiangchang mercury deposit. Sample/chondrite of Y axis means the ratio of rare earth elements in samples to those in C1 carbonaceous chondrite. **a** Chondrite-normalized REE pattern of the sample of SXC-9. SXC-9-1 represents the first cathode luminescence field of sample SXC-9. SXC-9-1-1 represents the first test point of the first cathode luminescence field of sample SXC-9 (Fig. 5a). The rare earth partition numbers in other figures are similar to this. **b** Chondrite-normalized REE pattern of the sample of SXC-9. **c** Chondrite-normalized REE pattern of the sample of SXC-5. **d** Chondrite-normalized REE pattern of the sample of SXC-1. **e** Chondrite-normalized REE pattern of the sample of SXC-23. **f** Chondrite-normalized REE pattern of the sample of SXC-23

homogenization temperatures are 150 °C (Table 1). Calcite fluid inclusion homogenization temperature data are shown in the literature (Huang and Du 1993; Li et al. 2002, 2013; Li and Zhou 1988). The $\delta^{13}C$ value of carbon dioxide is calculated to be in the range of − 3.46 ∼ − 1.42 ‰ in Dol 1 stage dolomite, − 7.84 ∼ − 3.22 ‰ in Dol 2 stage dolomite, and − 7.08 ‰ in Cal 2 stage calcite. According to the calcite-fluid oxygen isotope conversion formula: $1000 \ln \alpha = 2.78 \times 10^6/T^2 - 3.39$ (T = 0–500 °C) (O'Neil et al. 1969), and calcite fluid inclusion homogenization temperature data. The calcite oxygen isotope can be converted into the fluid oxygen isotopic value. $1000 \ln \alpha = \delta^{18}O_{CaCO_3} - \delta^{18}O_{H_2O}$, T representative Kelvin temperature. The calculated result is as follows: the $\delta^{18}O$ value of fluid oxygen to be in the range of 4.77–12.25 ‰ in Dol 1 stage dolomite, 3.63–10.96 ‰ in Dol 2 stage dolomite, and − 6.08 ‰ in Cal 2 stage calcite.

5.4 S isotope of cinnabar

In this experiment, we selected 17 cinnabar samples for sulfur isotope analysis, in which cinnabar was symbiotic with calcite and dolomite. The range of $\delta^{34}S$ is 12.08–24.28 ‰ (Table 2). For one cinnabar sample with symbiotic host-rock, $\delta^{34}S$ is 12.08 ‰. While for other samples, $\delta^{34}S$ are mainly above 20.00 ‰.

6 Discussion

6.1 Carbonate mineral trace elements and REEs concentration implications on the ore-forming fluid property

In our study, we find that in dolomite, the area that glows bright red tends to have a higher content of Mn and a lower content of Fe (Fig. 5e, points 2 and 3), and the area that glows dark red tends to have a lower content of Mn and a higher content of Fe (Fig. 5e, points 1 and 4). The average concentrations of Al, As, Mo, Sb, and Sr in Dol 1 stage dolomite are lower than Dol 2 stage dolomite. This indicates that the fluid enriched these elements more in the late metallogenic period. The average concentrations of As, Cu, Si, Sn, and Sr in Cal 2 stage calcite are higher than Dol 1 and Dol 2 stages of dolomite. This indicates that these elements are easier access to calcite.

REEs are of particular interest in geoscience due to their use as chemical tracers of natural processes. As a result of their systematic electron configuration, they exhibit

relatively similar chemical behavior. Their gradually varying ionic size, however, leads to distinct REE concentration patterns stemming from their aqueous complexation and their varying ability to incorporate into and/or adsorb onto solid phases (Möller et al. 1991, 2003; Möller 1997, 2002).

In our study, the Dol 1 stage massive dolomite partition curve exhibits light REE enrichment. This REE distribution is the same as that of the host-rock (Zhuo et al. unpublished data). The Dol 2 stage dolomite vein and Cal 2 stage calcite vein symbiosis with cinnabar partition curve show a flat-type (Fig. 8c–f). In the Dol 2 stage dolomite, there is a strongly Eu negative anomaly (Fig. 8d, e). The type of the REE partition curve indicates that the ore-forming fluid in Dol 1 stage dolomite is closer to the characteristics of the host-rock and the reaction degree between the fluid and host-rock in the early mineralization stage is greater than late mineralization stage. The negative anomaly of Eu indicates the late ore-forming fluid is oxidized. The Dol 2 stage dolomite and Cal 2 stage calcite are both vein-shaped, and their REE distributions are both flat. Dol 2 stage dolomite shows an obvious Eu negative anomaly. These phenomena indicate that in the late metallogenic period, the fluid is more concentrated in heavy REE, and the metallogenic environment is more oxidized.

6.2 Carbon and oxygen isotope composition implications on the source of C and O

The carbon and oxygen isotopes composition of calcite and dolomite of hydrothermal ore deposits can provide important constraints on the origin of mineralizing fluids, alteration temperature, and size of a hydrothermal system (Zheng and Hoefs 1993). In our study, the $\delta^{18}O$ values were in the range of 13.80–21.27 ‰ and 15.77–23.09 ‰ for Dol 1 and Dol 2 stage dolomite, and 4.77–12.25 ‰ and 3.63–10.96 ‰ for converted fluid $\delta^{18}O$ values, respectively (Table 1). This indicates that the H_2O of the mineralization fluid of the Sixiangchang mercury deposit is mainly from the dissolution of marine carbonate and mixes with H_2O of sedimentary organic matter decarboxylation (Fig. 9). The $\delta^{13}C$ values ranged from − 4.21 to − 2.16 ‰ and − 6.89 to − 2.27 ‰ for Dol 1 and Dol 2 stage dolomite, and − 3.46 to − 1.42 ‰ and − 7.84 to − 3.22 ‰ for converted fluid $\delta^{13}C$ of carbon dioxide, respectively. This indicates that the mineralization of CO_2 mainly comes from mantle degassing and sedimentary organic matter decarboxylation (Fig. 9). Therefore, $\delta^{13}C$ and $\delta^{18}O$ of calcite and dolomite indicate that the ore-forming fluid is mainly dominated by the dissolution of marine carbonate and the decarboxylation of sedimentary organic matter.

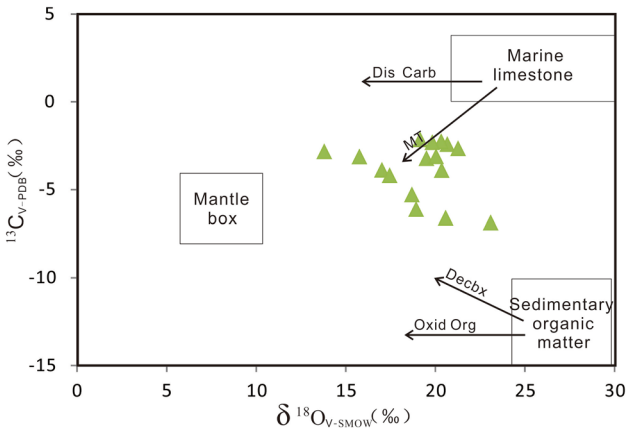

Fig. 9 Scheme diagram of the fluid source of Sixiangchang mercury deposit. The arrows show typical isotopic trends resulting from carbonate dissolution (Dis Carb), mixture (MT), decarboxylation of organic matter (Decbx), and the oxidation of organic matter (Oxid Org) [fields of mantle reservoir according to Hoefs (1997), Demény et al. (2004); sedimentary marine carbonates reservoir according to Veizer et al. (1999), typical isotopic trends according to Hu et al. (2017)]

6.3 Possible origins of sulfur

The $\delta^{34}S$ values of cinnabar showed a narrow range of 16.51–24.28 ‰, excluding one sample which had a $\delta^{34}S$ value of 12.08 ‰ (Table 2). The strong local fluid-rock interaction experienced by sulfur between the formation water and the host-rock during fluid transport can affect the cinnabar sulfur isotope composition. The $\delta^{34}S$ values of sulfide minerals are not always equal to that of the hydrothermal fluids from which they precipitated and are controlled by the physical and chemical conditions during the transport of hydrothermal fluids and precipitation of related minerals, namely, the total sulfur composition, temperature, oxygen fugacity (f_{O_2}), pH, and ionic strength (Ohmoto 1972). In the Sixiangchang deposit area, contemporaneous (Cambrian–Ordovician) seawater sulfate $\delta^{34}S$ is about 30 ‰ (Yan et al. 1989; Chang et al. 2008) (Fig. 10). There are three distinct reservoirs of $\delta^{34}S$ (Rollinson 1993): (1) mantle-derived sulfur with $\delta^{34}S$ value of 0 ‰ ± 3 ‰ (Chaussidon et al. 1989), (2) seawater sulfur with $\delta^{34}S$ value of 20 ‰ today, though this value has varied in the past, and (3) strongly reduced (sedimentary) sulfur with large negative $\delta^{34}S$ values. The $\delta^{34}S$ we measured to be less than the contemporaneous seawater sulfate $\delta^{34}S$ value, which is mainly related to the participation of $\delta^{32}S$ bio-sulfur in the ore-forming fluid. Our data and these phenomena indicate that the sulfur mainly comes from the host-rock (Cambrian strata) and is deposited into the area.

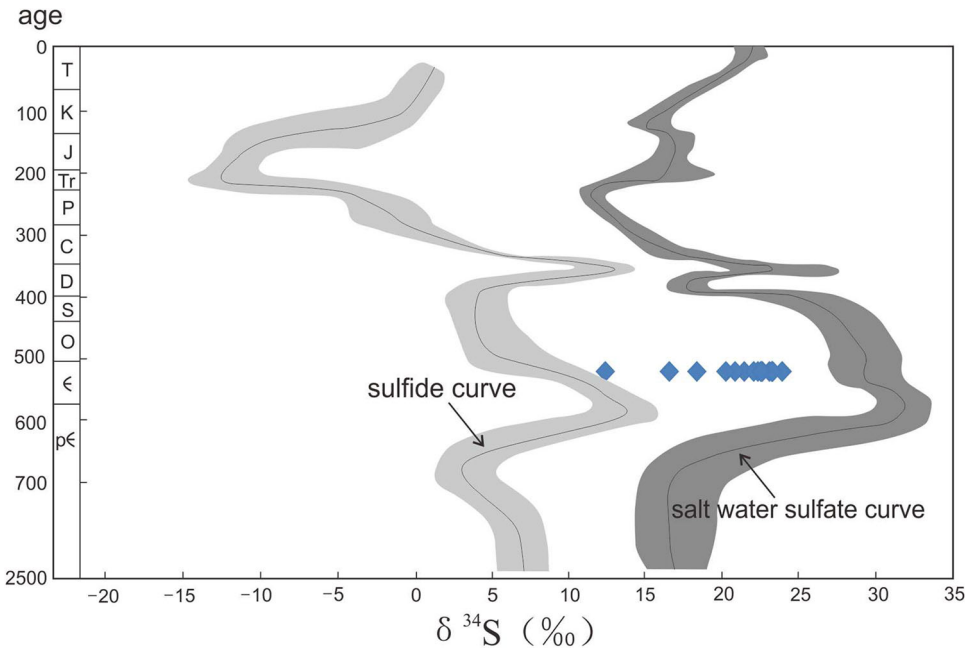

Fig. 10 Diagram of the cinnabar sulfur $\delta^{34}S$ of Sixiangchang mercury deposit. Blue solid point is our $\delta^{34}S$ data. Variation of S isotopic through geologic time diagram. Modified from Chang et al. (2008)

6.4 Sources and properties of ore-forming fluid

In summary, according to dolomite and calcite $\delta^{13}C$ and $\delta^{18}O$ data, carbon and oxygen of carbonate minerals in Sixiangchang mercury deposit are the dissolution of marine carbonate and the decarboxylation of sedimentary organic matter. The ore-forming fluid is mainly heated recycling groundwater that was recharged by meteoric water. This groundwater may come from the deep crustal, because the carbon isotope composition of carbon dioxide in the ore-forming fluid shows the characteristics of mantle carbon isotope composition. According to the result of REE concentration, the ore-forming fluids were reduced at the early stage, and gradually became oxidized with the progress of ore-forming. The sulfur isotope result showed that the sulfur is derived mainly of seawater sulfate with the participation of microbial reduction. Sulfur is sedimentary in origin, originating primarily from the host-rock strata.

7 Conclusions

Based on our study of the cathode luminescence characteristics of different stages of calcite and dolomite, trace elements and REEs, carbon and oxygen isotopes composition, and sulfur isotope composition of cinnabar, we can draw the following conclusions.

1. The Cal 2 stage calcite and Dol 2 stage dolomite exhibited a flat-type REE partition curve, and Dol 2 dolomite showed a strong negative anomaly for Eu. The REE partition curve of Dol 1 stage dolomite showed a trend of light REE enrichment.
2. Carbon and oxygen isotopes and trace elements data of dolomite and calcite indicate that, with the progress of mineralization, Al, As, Mo, Sb, and Sr were gradually enriched in the ore-forming fluid. The early ore-forming fluid was reduced, and the late ore-forming fluid was oxidized. The ore-forming fluid of the deposit was a mixture of deep crustal fluid and meteoric water in deep thermal circulation, and was involved in the oxidation of organic matter.
3. Cinnabar sulfur isotope results showed that the sulfur was primarily derived from seawater sulfate with the participation of microbial reduction. Sulfur is sedimentary in origin, derived mainly from the host-rock (Cambrian strata).

Acknowledgements This study was funded by the National 973 Program of China (2014CB440906) and the key project of the National Natural Science Foundation of China (41230316). We thank Dai Zhihui and Tang Yanwen for LA-ICP-MS analysis, Gu Jing for C, O and S isotopes analysis.

References

Bao YM, Wan RJ, Bao ZX (1999) Discussion of the mercury mineralization related to the mercury metallogeic belt of Hunan-Guizhou province. Beijing Geol 2:5–12 **(in Chinese with English abstract)**

Chacko T, Mayeda TK, Clayton RN, Goldsmith JR (1991) Oxygen and carbon isotope fractionations between CO_2 and calcite. Geochim Cosmochim Acta 55(10):2867–2882

Chang ZS, Large RR, Maslennikov V (2008) Sulfur isotopes in sediment-hosted orogenic gold deposits: evidence for an early timing and a seawater sulfur source. Geology 36(12):971–974

Chaussidon M, Albare F, Sheppard SM (1989) Sulphur isotope variations in the mantle from ion microprobe analyses of microsulphide inclusions. Earth Planet Sci Lett 92(2):144–156

Chen L, Liu YS, Hu ZC, Gao S, Zong KQ, Chen HH (2011) Accurate determinations of fifty–four major and trace elements in carbonate by LA-ICP-MS using normalization strategy of bulk components as 100%. Chem Geol 284:283–295

Demény A, Sitnikov M, Karchevsky P (2004) Stable C and O isotope compositions of carbonatite complexes of the Kola Alkaline Province: phoscorite-carbonatite relationships and source compositions. In: Wall F, Zaitsev AN (eds) Phoscorites and carbonatites from mantle to mine: the key example of the Kola Alkaline Province. Mineral Soc, London, pp 407–431

Du YS, Huang H, Yang JH, Huang HW, Tao P, Huang ZQ, Hu LS, Xie CX (2013) The basin translation from Late Paleozoic to Triassic of the Youjiang basin and its tectonic signification. Geol Rev 59:1–11 **(in Chinese with English abstract)**

Friedman L, O'Neil JR (1977) Compilation of stable isotope fractionation factors of geochemical interest. In: Fleischer M (ed) Data of geochemistry, sixth edn. Geological Survey Professional Paper, Reaton, VA, vol 440-KK, pp KK1–KK12Han ZC

He LX (1990) The forming condition and existing regularity of Au mineralization in Hg ore belt. Geol Guizhou 7(3):187–195 **(in Chinese with English abstract)**

Hoefs J (1997) Stable isotope geochemistry. Springer, Berlin

Hu RZ, Zhou MF (2012) Multiple Mesozoic mineralization events in South China-an introduction to the thematic issue. Mineral Deposita 47:579–588

Hu RZ, Su WC, Bi XW, Tu GZ, Hofstra AH (2002) Geology and geochemistry of Carlin-type gold deposits in China. Miner Deposita 37:378–392

Hu RZ, Fu SL, Huang Y, Zhou MF, Fu SH, Zhao CH, Wang YJ, Bi XW, Xiao JF (2017) The giant South China Mesozoic low-temperature metallogenic domain-reviews and a new geodynamic model. J Asian Earth Sci 137:9–34

Huang GS, Du YY (1993) The features and genesis of micrograined and disseminated gold deposit in Shan Dan Hg-ore zone. Geol Guizhou 34(1):1–9 **(in Chinese with English abstract)**

Jia RF, Chen QN, Zhou PK, Xia Y, Wu XY (1993) Relation between Au-enrichment periods and organic matter in Danzhai gold deposit Guizhou. Contrib Geol Miner Resour Res 8(4):69–81 **(in Chinese with English abstract)**

Jochum KP, Scholz D, Stoll B (2012) Accurate trace element analysis of speleothems and biogenic calcium carbonates by LA-ICP-MS. Chem Geol 2012:318–319

Jochum KP, Weis U, Stoll B, Kuzmin D, Jacob DE, Stracke A, Birbaum K, Frick DA, Günther D, Enzweiler J (2015) Determination of reference values for NIST SRM 610-617 glasses following ISO guidelines. Geostand Geoanal Res 35:397–429

Lei YJ, Dai YP, Duan QF, Wang GQ, Zhao WQ (2012) Rotational shear tectonics and metallogeny of the of the mercury ore belt in Hunan and Guizhou Provinces, China. Geotectonic et Metallogenia 36(4):525–529

Li ZZ, Zhou DK (1988) Diagenesis of mercury ore zone in Tongren-Fenghuang-Sandu-Danzhai region. Oil Gas Geol 9(4):428–435

Li HY, Gao ZM, Yang ZS, Luo TY, Rao WB (2002) Geochemical features of Danzhai Carlin-type gold deposit, Guizhou Province. Chin J Geol 37(1):1–7 **(in Chinese with English abstract)**

Li BH, Li WW, Gu XX, Xiao DC, Huang ZB, Cheng WB, Chen CH, Dong SY (2013) A study of methane inclusion of the Danzhai mercury ore field in Guizhou Province and its geological significance. Earth Sci Front 20(1):55–63 **(in Chinese with English abstract)**

Liu YS, Hu ZC, Gao S, Günther D, Xu J, Gao CG, Chen HH (2008) In situ analysis of major and trace elements of anhydrous minerals by LA-ICP-MS without applying an internal standard. Chem Geol 257:34–43

Liu YS, Hu ZC, Zong KQ (2010) Reappraisement and refinement of zircon U-Pb isotope and trace element analyses by LA-ICP-MS. Chin Sci Bull 55(15):1535–1546 **(in Chinese with English abstract)**

Möller P (1997) Rare earth element and yttrium fractionation caused by fluid migration. Geoscience 42:43

Möller P (2002) Rare earth elements and yttrium in geothermal fluids. Water Sci Technol Libr 40:97–125

Möller P, Lüders V, Schröder J, Luck J (1991) Element partitioning in calcite as a function of solution flow rate: a study on vein calcites from the Harz Mountains. Miner Deposita 26:175–179

Möller P, Dulski P, Morteani G (2003) Partitioning of rare earth elements, yttrium, and some major elements among source rocks, liquid and vapor of Larderello-Travale geothermal field, Tuscany (Central Italy). Geochim Cosmochim Acta 67:171–183

O'Neil JR, Clayton RN, Mayeda TK (1969) Oxygen isotope fractionation in divalent metal carbonates. Chem Phys 51(12):5547–5558

Ohmoto H (1972) Systematics of sulfur and carbon isotopes in hydrothermal ore deposit. Econ Geol 67:551–578

Robinson BW, Kusakabe M (1975) Quantitative preparation of sulfur dioxide, for $^{34}S/^{32}S$ analyses, from sulfides by combustion with cuprous oxide. Anal Chem 47(7):1179–1181

Rollinson HR (1993) Using geochemical data: evaluation, presentation, interpretation. Longman Scientific and Technical, Copublished in the U.S. with J. Wiley and Sonswenle

Rytuba JJ (2003) Mercury from mineral deposits and potential environmental impact. Environ Geol 43(3):326–338

Saupe F (1990) Geology of the Almaden mercury deposit, Province of ciudad real, Spain. Econ Geol 85(3):482–510

Shi JX (1991) On the relationship between organic matter and mercury mineralization in eastern guizhou in special reference to organic inclusion data. Acta Mineral Sinica 11(4):341–345 **(in Chinese with English abstract)**

Su WC, Xia B, Zhang H, Zhang XC, Hu RZ (2008) Visible gold in arsenian pyrite at the Shuiyindong Carlin-type gold deposit, Guizhou, China: implications for the environment and processes of ore formation. Ore Geol Rev 33:667–679

Su WC, Heinrich CA, Pettke T, Zhang XC, Hu HR, Xia B (2009) Sediment-hosted gold deposits in Guizhou, China: products of wall-rock sulfidation by deep crustal fluids. Econ Geol 104:73–93

Su WC, Zhang HT, Hu RZ, Ge X, Xia B, Chen YY, Zhu C (2012) Mineralogy and geochemistry of gold-bearing arsenian pyrite from the Shuiyindong Carlin-type gold deposit, Guizhou, China: implications for gold depositional processes. Miner Deposita 47(6):653–662

Su WC, Dong WD, Zhang XC, Shen NP, Hu RZ, Albert H, Cheng LZ, Xia Y, Yang KY (2018) Carlin-type gold deposits in the dian-qian-gui "golden triangle" of southwest China. Rev Econ Geol 20:157–185

Veizer J, Ala D, Azmy K, Bruckschen P, Buhl D, Bruhn F, Carden GAF, Diener A, Ebneth S, Godderis Y (1999) $^{87}Sr/^{86}Sr$, $\delta^{13}C$, and $\delta^{18}O_{V\text{-}SMOW}$ evolution of Phanerozoic seawater. Chem Geol 161:1586

Wang JS, Gao ZH (2017) Geochemical characteristics and implications of REE, carbon and oxygen isotopes of calcite from La'e Mercury Deposit. J Kunming Univ Sci Technol 42(3):28–37 **(in Chinese with English abstract)**

Wang JS, Wen HJ (2015) Sm-Nd dating of hydrothermal calcites from JiaoLi-Lae Mercury deposit, Guizhou Province. J Jilin Univ Earth Sci Ed 45(5):1384–1393 **(in Chinese with English abstract)**

Wang ZH, Chen JB, Feng XB, Hintelmann Holger, Yuan SL, Cai HM, Huang Q, Wang SX, Wang FY (2015) Mass-dependent and mass-independent fractionation of mercury isotopes in precipitation from Guiyang, SW China. CR Geosci 347:358–367

Wei AY, Xue CD, Xiang K, Li J, Liao C, Qureshi JA (2015) The ore-forming process of the Maoping Pb–Zn deposit, northeastern Yunnan, China: constraints from cathodoluminescence (CL) petrography of hydrothermal dolomite. Ore Geol Rev 70:562–577

Xie ZJ, Xia Y, Yan BW, Wang ZP, Tan QP, Wu SR, Fan RC (2014) Geochemical characteristics and metallognic materials source of Carlin-type gold deposits in the Sandu-Danzhai metallogenic zone, Guizhou. Bull Mineral Petrol Geochem 33(3):326–333 **(in Chinese with English abstract)**

Yan JP, Yang KW, Wang HY, Zeng RL, Ding LX, Li Q, Li LY, Xiang MM, Huang CL (1989) Mercury deposits in guizhou. Geological Publishing House, Beijing, pp 1–366 **in Chinese with English abstract**

Zheng YF, Hoefs J (1993) Carbon and oxygen isotopic covariations in hydrothermal calcites. Miner Deposita 28:79–89

Zhou ZB, Wen HJ, Qin CJ, Liu L (2017) Geochemical and isotopic evidence for a magmatic-hydrothermal origin of the polymetallic vein-type Zn–Pb deposits in the northwest margin of Jiangnan Orogen, South China. Ore Geol Rev 86:673–691